Synthesis of minerals

Yamnova N.A., Gurbanova O.V., Borovikova E.Yu., Volkov A.S., Dimitrova O.V. Synthesis, crystal structure features, IR-spectrocopy and properties of natural calcium metaborates synthetic analogs and new Na,Ca carbonate–borate.

MSU, Faculty of Geology, Moscow (natalia-yamnova@yandex.ru)

Abstract. The hexahydroborite analog $Ca[B(OH)_4]_2 \cdot 2H_2O$ **(I)**, fabianite dimorph synthetic $CaB_3O_5(OH)$ **(II)**, and new Ca,Na-carbonate-borate $Ca_2Na(Na_xCa_{0.5-x})[(OH)(O_{1-x}OH_x)](CO_3)(x{\sim}0.4)$ **(III)** have been synthesized by the hydrothermal method at t = 250°C and P = 70–80 atm: (I) via the recrystallization of calciborite CaB_2O_4 (M) in the system $M–B_2O_3–H_2O$, (II,III) in the system $Ca(OH)_2–H_3BO_3–Na_2CO_3–NaCl$. The crystal structures of three borates were refined by the least-squares method with anisotropic displacement parameters (H atoms were located) and final R_1 = 0.0260(I), 0.0428(II), 0.0387(III).

Keywords:calcium metaborate, hydrothermal method, hexahydroborate, fabianite, carbonate-borate, nonlinear-optical properties

The hexahydroborite analog [1]$Ca[B(OH)_4]_2 \cdot 2H_2O$ **(I)**, fabianite dimorph synthetic Ca triborate [2]$CaB_3O_5(OH)$ **(II)** and new [3]Ca,Na-carbonate-borate $Ca_2Na(Na_xCa_{0.5-x})[(OH)(O_{1-x}OH_x)](CO_3)(x{\sim}0.4)$ **(III)** have been synthesized by the hydrothermal method (*t* = 250°C, *P* = 70–80 atm): (I) via the recrystallization of calciborite CaB_2O_4 (*M*) in the system $M–B_2O_3–H_2O$; **(II,III)** in the system $Ca(OH)_2–H_3BO_3–Na_2CO_3–NaCl$. The crystal structures of three borates (autodiffractometer Xcalibur S CCD, λMoKα) were refined by the least-squares method in the anisotropic displacement parameters (H atoms were located) and final R_1:

(I) 0.0260, 1196 reflections with I > 2σ(I);
(II) 0.0428, 972 reflections with I> 2σ(I);
(III) 0.0387, 2663 reflections with I> 2σ(I).

The structure of synthetic hexahydroborite $Ca[B(OH)_4]_2 \cdot 2H_2O$ (*a*=7.9941(3), *b*=6.6321(2), *c*=7.9871(3) Å, *β*=104.166(4)°, *V* = 410.58(3) Å^3, sp.gr. *P2/c*, Z=2, ρ_{calc}=1.89 g/sm^3) consists of infinite columns running along the *c* axis. The columns are formed by Ca polyhedra linked together and to $[B(OH)_4]$ orthotetrahedra by sharing edges. Along the two other axes, the translationally equivalent columns are linked only by hydrogen bond (Fig.1a,b). Anhydrous calciborite CaB_2O_4 and synthetic analog of hexahydroborite $Ca[B(OH)_4]_2 \cdot 2H_2O$ are the end members of series of borates with the general chemical formula $CaB_2O_4 \cdot nH_2O$ (n = 0–6) with the constant CaO : B_2O_3 = 1 : 1 ratio and variable content of water.

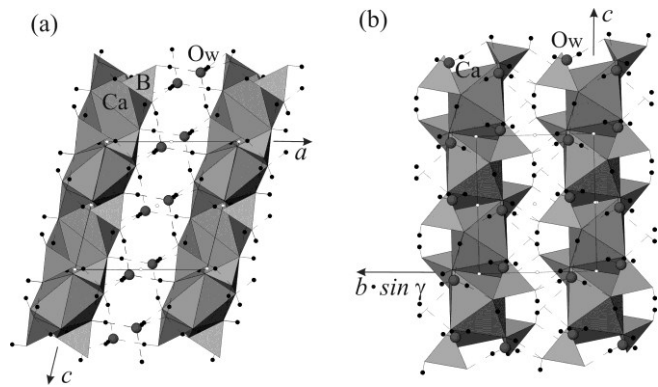**Fig. 1. Structure of the synthetic hexahydroborite analog $Ca[B(OH)_4]_2 \cdot 2H_2O$ projected onto** the (a) *xz* and (b) *yz* planes. The *D*–H and H⋯⋯*A* bonds are indicated by solid and dashed lines, respectively. The centers of inversion are represented as small white circles.

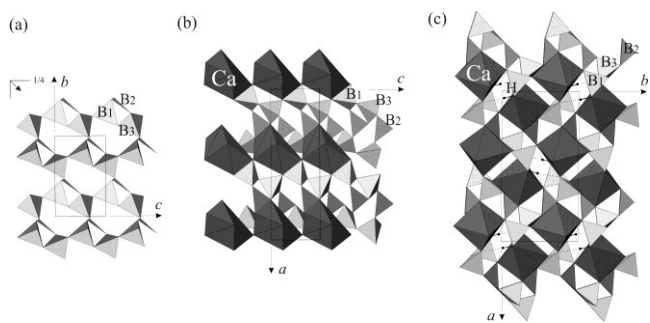**Fig. 2. Structure of the synthetic Ca triborate $CaB_3O_5(OH)$ (III):** (a) projection of a boron–oxygen layer onto the *yz* plane; side view of boron–oxygen layers and columns of seven-vertex polyhedra of Ca in the projection onto the *xz* plane (b) and *xy* plane (c).

Corrugated layers (100) formed by BO_4 tetrahedra and BO_3 triangles are the base of the synthetic Ca triborate $CaB_3O_5(OH)$ structure (*a*=13.490(1), *b*=6.9576(3), *c*=4.3930(2) Å, *V*=412.32(3)Å^3, sp.gr. *Pna2$_1$*, Z=4, ρ_{calc}=2.731 g/sm^3). These layers are built of pentaborate radicals 5(2Δ + 3T) which form colemanite type chains running along the diagonal of the *bc* face of the unit cell (Fig. 2a). The colemanite chains that are related by the translation along the shortest direction (the *c* axis equal to ~4.4 A) share vertices of two BO_4 tetrahedra to form a layer. In the same direction, pyroxene-type chains of BO_4 tetrahedra are formed (Fig. 2b). Columns of seven-vertex Ca polyhedra, which fill voids between corrugated boron–oxygen layers and connect neighboring layers along the *a* axis, are stretched parallel to the pyroxene-like chains along the *c* axis (Fig. 2c). $CaB_3O_5(OH)$ is the

member of a series of borates with the general chemical formula $Ca_2B_6O_{11} \cdot nH_2O$ ($n = 0$–13) with the constant $CaO : B_2O_3 = 2 : 3$ ratio and variable content of water. Among the compounds of this series, the structure of Ca triborate studied in this work is comparable with that of its formula analogue, natural borate fabianite $CaB_3O_5(OH)$. The study of the nonlinear-optical properties for the fabianite dimorph $CaB_3O_5(OH)$ **(II)** showed the SHG signal exceeding that of the quartz standard. Calcium triborate $CaB_3O_5(OH)$ on heating turns to centrosymmetric calciborite $2xCaB_2O_4=Ca_2[BO_3BO]_2$.
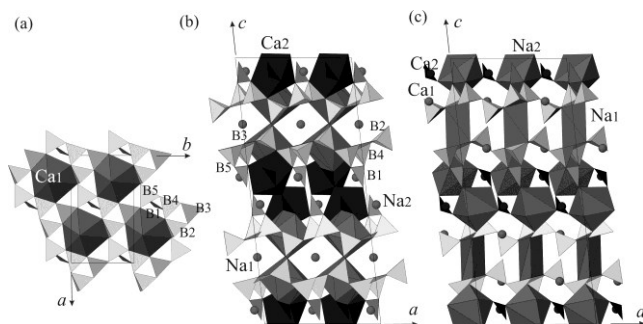

Fig. 3. Structure of the Ca,Na carbonate–borate: (a) boron–oxygen layer with Ca1 nine-vertex polyhedra in the *xy* projection; (b, c) architecture of cation structures in the *xz* projection from (b) Ca polyhedra and (c) Na polyhedra. Black isolated triangles show CO_3 groups.

The structure of new Ca,Na-carbonate-borate $Ca_2Na(Na_xCa_{0.5-x})$ $[B^t_3B^\Delta_2O_8(OH)(O_{1-x}OH_x)](CO_3)$ ($a = 11.1848(3)$, $b = 6.4727(2)$, $c = 25.8181(7)$Å, $\beta = 96.364(3)°$, $V = 1857.60(9)$Å^3, sp.gr. $C2/c$, $Z = 8$, $\rho_{calc} = 2.801$ g/sm^3) based on boron–oxygen corrugated layers (001) formed by pentaborate radicals $5(2\Delta+3T)$ $[B^t_3B^\Delta_2O_8(OH)(O,OH)]$ (Fig.3a). Ca and Na polyhedra and CO_3 triangles are located between the layers (Fig. 3b, c). A crystallochemical analysis of new Ca,Na carbonate–borate has established its similarity to natural Na,Ca pentaborates (heidornite $Na_2Ca_3[B_5O_8(OH)_2]\cdot2SO_4\cdot Cl$ and tuzlaite $NaCa[B_5O_8(OH)_2]\cdot3H_2O$) and synthetic Na,Ba-decaborate $Na_2Ba_2[B_{10}O_{17}(OH)_2]$.

The presence of OH−groups and water molecules in the crystals of the synthetic hexahydroborite analog $Ca[B(OH)_4]_2 \cdot 2H_2O$ as well as the presence of isolated CO_3–groups and OH−groups in the crystals of the Ca,Na carbonate–borate were confirmed by IR spectroscopy. The IR spectrum was recorded on FSP1201 Fourier spectrometer using standard KBr disk technique. The IR spectrum of synthetic hexahydroborite was contributed to the [4]RRUFF Project database.

With increasing water content, the density of compounds of diborate series $CaB_2O_4 \cdot nH2O$ ($n = 0$–

6) and triborate series $Ca_2B_6O_{11} \cdot nH_2O$ ($n = 0$–13) decreases regularly. The synthetic analogue of [1]hexahydroborite is the product of recrystallization of calciborite. Both compounds are the end members of the first series. Ca triborate (**II**) $CaB_3O_5(OH)$ described [5]early was obtained by calcination of inyoite $CaB_3O_3(OH)_5 \cdot 4H_2O$ ($n = 13$), i.e., the end member of the triborate series considered in this work. These transformations testify that phase transitions can take place in both borate series. The transition of calcium triborate $CaB_3O_5(OH)$ on heating to centrosymmetric calciborite $Ca_2[BO_3BO]_2$ is indicative of phase relationships between the members of different series: $CaB_2O_4 \cdot nH_2O$ ($CaO:B_2O_3=1:1$) diborates and $Ca_2B_6O_{11} \cdot nH_2O$ ($CaO:B2O3=2:3$) triborates.

References:

1. N. A. Yamnova, E. Yu. Borovikova, and O. V. Dimitrova // Crystallography Reports, 2011, Vol. 56, No. 6, pp. 1079–1084.
2. N. A. Yamnova, S. M. Aksenov, S. Yu. Stefanovich, A. S. Volkov, and O. V. Dimitrova// Crystallography Reports, 2015, Vol. 60, No. 5, pp. 649–655.
3. N. A. Yamnova, E. Yu. Borovikova, O. A. Gurbanova, O. V. Dimitrova, and N. V. Zubkova // Crystallography Reports, 2012, Vol. 57, No. 3, pp. 381–387.
4. R. T. Downs, The RRUFF Project: an integrated study of the chemistry, crystallography, Raman and infrared spectroscopy of minerals. Program and Abstracts of the 19th General Meeting of the International Mineralogical Association, Kobe, Japan, 2006, p. O03.
5. J. R. Clark, C. L. Christ, and D. E. Appleman // Acta Crystallographica, 1962, Vol.15, pp. 207-211

Sinyakova E.F., Kosyakov V.I. Types of platinum-bearing pentlandite in the Cu-Fe-Ni-S system

V. S. Sobolev Institute of Geology and Mineralogy SB RAS, Novosibirsk (efsin@igm.nsc.ru), A. V. Nicolaev Institute of Inorganic Chemistry SB RAS, Novosibirsk (kosyakov@niic.nsc.ru)

Abstract. An experimental simulation of the pentlandite formation during one-dimensional crystallization of the Cu-Fe-Ni-S-(Pd, Rh, Ir, Ru) melts was performed. The crystallized samples consisted of pyrrhotite, pentlandite, chalcopyrite, haycockite, mooihoekite, bornite and unknown phase $\Sigma(Fe+Ni+Cu)/S = 11/9$. Four types of pentlandite with different cationic ratio were found. The position of these types in the concentration tetrahedron Cu-Fe-Ni-S system was located. It was shown that Pd, Rh, Ir and Ru formed solid solutions with pentlandite. These PGE are not indicators of types of pentlandite, but may point at possible mechanisms of their formation.

Pentlandite $(Fe_zNi_uCu_{1-z-u})_{9+\delta}S_8$ (*pn*) is one of the widespread minerals in zonal massive ores of magmatogene Pt-Cu-Ni deposits. It is one of the main concentrators of platinum group elements (PGE). In [Kullerud et al., 1969; Fedorova, Sinyakova, 1993] the authors assumed that in the Fe-Ni-S system *pn* may appear as a product of a solid phase reaction at temperatures below 615°C. It was shown [Craig, Kullerud, 1969; Peregoedova et al., 1995] that pentlandite can be present in the Cu-Fe-Ni-S system. In [Sinyakova, Kosyakov, 2007] it was assumed, that pentlandite-bornite eutectic can be formed from the melt in the Fe-Cu-Ni-S system. On the basis of our own and literature data we came to a conclusion, that pentlandite formed several forms with different ability to accumulate PGE.

To determine the regions of existence of pentlandite types in the Cu-Fe-Ni-S system and the mechanism of their formation additional investigation of phase relations in this system were carried out by the quasi-equilibrium directional solidification. This method allows to continuously scan the compositions of solid phases or phase associations, crystallized from the melt along the trajectories of melt composition. This peculiarity of the process allows to determine the possibility of crystallization of *pn* from the melt, or as a result of solid-state reactions at low temperatures.

One-dimensional crystallization of the melts with composition of (mol.%) .%): Cu 11.8, Fe 23.3, Ni 17.5, S 47.0, Pt, Pd, and Rh 0.2 each (sample I), Cu 16.8, Fe 18.7, Ni 19.3, S 44.2, Pt, Pd, Rh, Ru, and Ir 0.2 each (sample II), Cu 24.03, Fe 22.25, Ni 4.34, S 47.08, Pt, Pd, Rh, Ru, and Ir 0.2 each (sample III) was carried out by the vertical Bridgman method. The ampoule with homogenous melt had been dropped from the hot zone to the cold one at 2.3×10^{-8} m/s rate. Lengths of cylindrical specimens were from 70 to 90 mm and their diameter was 7 mm. Ingots were cut into 17 disks, and each one was weighed to determine the mole fraction of crystallized melt (*g*). These disks were used to prepare polished sections. They were examined by means of microscopic, electron microprobe analyses, and X-ray diffraction.

Experimental results

Sample I includes three zones. The first one consists of primary *mss* $Fe_{29.7}Ni_{17.7}Cu_{1.5}Rh_{0.2}S_{50.9}$. On cooling, this solid solution partly decomposes to form lamellar inclusions of less than 1 μm size, probably of pentlandite. Zone II consists of primary solid solution $Fe_{18.0}Ni_{12.8}Cu_{25.7}Pd_{0.1}S_{43.4}$. On cooling It decays into secondary phases: bornite solid solution $Fe_{12.6}Ni_{0.3}Cu_{46.5}S_{40.6}$ (*bnss*), haycockite $Fe_{26.9}Ni_{2.0}Cu_{23.6}S_{47.5}$ (*hc*), and pentlandite $Fe_{22.2}Ni_{29.6}Cu_{1.4}Pd_{0.3}S_{46.5}$ (*pn*). In

zone III there was the eutectic consisting of *mss* $Fe_{12.5-20.0}Ni_{33.0-23.5}Cu_{1.5-3.5}Rh_{1.7-2.2}Pd_{0.2}S_{49.5-50.5}$ and *bnss* $Fe_{10.2}Ni_{0.7}Cu_{49.4}S_{39.7,}$ which crystallized from the melt.
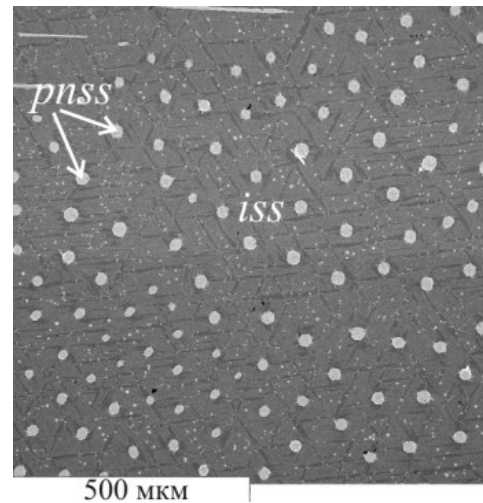

Fig. 1. Microstructure of zone III in sample II. Rounded inclusions of *pnss* in *iss* matrix.

Sample II consists of three zones. In zone I there was the eutectic mixture of *mss* $Fe_{12.5-20.0}Ni_{33.0-23.5}Cu_{1.5-3.5}Rh_{1.7-2.2}Pd_{0.2}S_{49.5-50.5}$ and *iss* $Fe_{26.0}Ni_{0.5}Cu_{23.5}S_{50.0}$ formed from the melt. Pentlandite inclusions appear on the borders of *mss* and *iss* in the cooling sample. A microstructure of zone II consists of rounded small inclusions (near 40 μm) of pentlandite solid solution $Fe_{10.5-11.0}Ni_{38.5}Cu_{1.1}Ir_{0.1}Pd_{0.2}Rh_{1.3-2.2}S_{47.7-48.4}$ (*pnss*) in the *iss* $Fe_{26.5-24.2}Ni_{0.5-1.5}Cu_{23.5-27.1}S_{47.6-48}$ matrix (Fig. 1). This indicates the formation of *pnss* from the melt. The observed microstructure is likely to be rod or globular eutectic. *Pnss* decomposes into *pn* $Fe_{13.2}Ni_{37.3}Cu_{0.9}Ir_{0.2}Rh_{1.3}S_{47.1}$ and Ni-*mss* $Fe_{9.0}Ni_{40.1}Cu_{0.5}Rh_{1.4}S_{49.0}$ on cooling. Between grains of *pnss* and *iss* there is a band consisting of *pn* $Fe_{21.2}Ni_{27.9}Cu_{3.5}Pd_{0.8}S_{46.6}$ and *bnss* $Fe_{13.0}Ni_{0.4}Cu_{45.3}S_{41.3}$. Primary *iss* decomposes into intergrowthes of the chalcopyrite $Fe_{25.0}Ni_{1.0}Cu_{25.0}S_{49.0}$ with other Fe-Cu-sulfides.

Sample III consists of six zones. Every zone represented a multiphase mix of decay products of primary phases. Primary phases were identified by means of the microscopic and chemical analysis. Pentlandite is present in all zones. The composition of pentlandite and its formation mechanism were determined by the microstructure and chemical analysis of samples from different areas of the ingot.

Fig. 2 shows a Me_9S_8 section of Cu-Fe-Ni-S concentration tetrahedron. The points show the cations relation in pentlandites presented in different samples. Additional unpublished authors' data and the data from [Peregoedova et al. 1995] are shown in this figure. The experimental points are grouped into

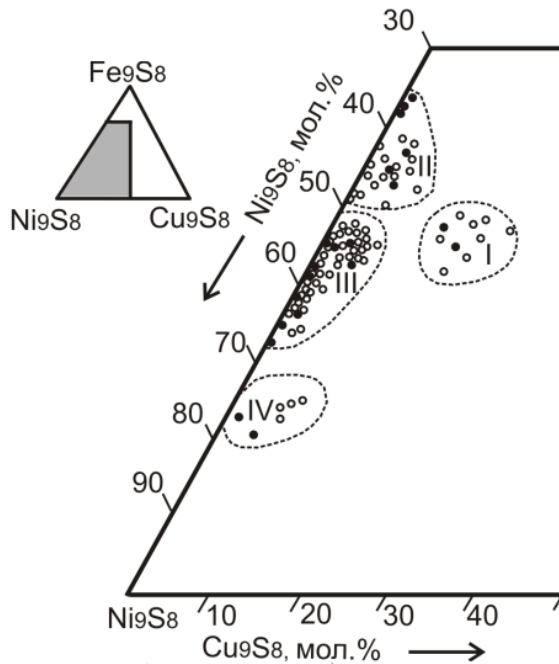four areas which correspond to four types of pentlandite.

Fig. 2. Arias of I - IV pentlandites in Me₉S₈ section of Cu-Fe-Ni-S system. Open circle is our data, close circle is data of [Peregoedova et al., 1995]

Type I is pentlandite enriched in Fe and Cu. It is present in the form of round grain of 200 μm to 1 mm size (sample III).

Type II is ferrous pentlandite with a low copper content. It exists in the form of micron lamellae in Fe-*mss*, Fe-*iss*, and as a border around the Fe-*mss* or intergrowths with bornite or bornite and haycockite.

The most common type of pentlandite is moderate Ni and poor Cu - type III. It is present as (a) microinclusions of Ni-*mss* and Ni-*iss*, (b) intergrowths with *hc* and *bnss*, (c) rims around Ni-*mss*, and (d) eutectic with *bnss* (samples II, III).

Type IV is the Ni-high rich pentlandite. It is present in the rod eutectic with *iss* (sample II) and in granular intergrowths with Cu-rich *bnss*.

Pentlandites of I, III and IV types are presented in the fragments of eutectic structures with *bnss* and *iss*, i.e. they can be in equilibrium with the quaternary melt. Such primary phases of pentlandite dissolve impurities of Pd, Rh, Ru, and Ir well, but Pt content in them is below the detection limit. Pentlandite II is a decay product. Pentlandite III and IV can be formed from the melt as well as a result of solid state reactions.

Pentlandite grains can be formed in different ways. Depending on their origin, they absorb different PGE and can containing one impurity (Rh or Pd), two impurities (Ir + Rh, Pd + Rh), three impurities (Ru + Ir + Rh) or four impurities (Ru + Ir + Rh + Pd) simultaneously. These PGE are not indicators of the types of pentlandite, but can point at possible mechanisms of their formation.

References:

1. Craig J.R., Kullerud G. 1969. Econ. Geol. Monograph / Ed. Wilson H.D.B. v. 4. p. 344-358.
2. Fedorova Zh. N.., Sinyakova E.F.1993. Russian Geology and Geophysics, v. 34, No. 2, pp. 79-87.
3. Kullerud G. et al. 1969. Econ. Geol. Monograph. v. 4. p. 323-343.
4. Peregoedova A.V. et al. 1995. Russian Geology and Geophysics, v. 36, No. 3, pp. 91-98.
5. Sinyakova E.F., Kosyakov V.I. 2007. Electronic Scientific Information Journal "Vestnik Otdelenia nauk o Zemle RAN" № 1(25)′.